Supporting Information

Enhanced electron transfer in Fe–N–C catalysts for nitrobenzene reduction: From electrodes to functional materials

Biao Wei [a#], *Daoqing Liu* [a#], *Ran Peng* [a], *Yi Zhou* [b], *Qianwei Li* [a*], *Huazhang Zhao* [c,d*]

[a] China University of Petroleum, Beijing 102249, P.R. China

[b] School of Chemistry and Life Resources, Renmin University of China, Beijing, 100872, China

[c] Key Laboratory of Water and Sediment Sciences (Ministry of Education), College of Environmental Sciences and Engineering, Peking University, Beijing 100871, People's Republic of China

[d] Shanxi Laboratory for Yellow River, College of Environmental and Resource Sciences, Shanxi University, Taiyuan 030006, China

[#] Both authors contributed equally to this work.

*To whom correspondence should be addressed

qianweili@cup.edu.cn (Q.W. Li)

zhaohuazhang@pku.edu.cn (H.Z. Zhao)

This *Supporting Information* includes

Number of pages: 35

Number of Figures: 17

Number of Table: 4

Number of Scheme: 1

List of text, table and figures

observed during 1000 linear sweep voltammetry (LSV) cycles. (d) XRD patterns of the post-cycling Fe–N–C electrode. (Scan rate=50 mV/s, [Na_2SO_4]=50 mM, [NB]=100 mg/L).

Fig. S5. Adsorption of nitrobenzene (NB) by electrodes prepared from active carbons (ACs), nitrogen-doped porous carbons (NPCs), and Fe–N–C. (pH=6.1, $[NB]_0$=100 mg/L, $[Na_2SO_4]_0$=50 mM, T=298 K).

Fig. S6. Effect of iron content in Fe–N–C electrodes on the electrocatalytic performance of nitrobenzene (NB). (inset: pseudo-first-order kinetic fitting). Experimental conditions: pH=6.1, $[NB]_0$=100 mg/L, $[Na_2SO_4]_0$=50 mM, T=298 K.

Fig. S7. Structural and compositional characterization of FeNCs-500 catalyst. (a) XRD patterns, and (b) high-resolution N 1s XPS spectra.

Fig. S8. Electrochemical reduction performance of NB using different electrocatalysts at varying pH conditions. (a) NB removal efficiency and (b) kinetics with GR electrode; (c) NB removal efficiency and (d) kinetics with NPCs electrode. (T=298 K, $[NB]_0$=100 mg/L, $[Na_2SO_4]_0$=50 mM, potential=-1.0 V *vs*. Ag/AgCl).

Fig. S9. (a) Reduction efficiency of NB and (b) its pseudo-first-order rate constant (k_{obs}) ratio on the Fe–N–C cathode with different *t*-BuOH concentrations (Potential=-1.0 V *vs*. Ag/AgCl, T=298 K, $[NB]_0$=100 mg/L, $[Na_2SO_4]_0$=50 mM, electrolysis time=180 min).

Fig. S10. Morphological and elemental characterization of Fe–N–C/ZVI. (a and b) FE-SEM images, (c) EDS elemental distribution, and (d) EDS elemental mapping images of Fe–N–C/ZVI. The inset of (c) shows the chemical composition of the samples.

Fig. S11. XRD patterns of the Fe–N–C/ZVI composite as well as Fe (PDF#85-1410, yellow vertical line) and Fe_2O_3 (PDF#89-0597, black vertical line) as references.

Fig. S12. High-resolution XPS spectra of (a) survey scan, (b) Fe 2p, (c) O 1s, and (d) C 1s for the Fe–N–C/ZVI composite.

Fig. S13. Parametric optimization of Fe–N–C/ZVI composites for nitrobenzene (NB) degradation. (a) Effect of mZVI/Fe–N–C mass ratio ([dosage]=1.0 g/L, ball-milling time: 4 h), (b) Ball-milling duration ([dosage]=1.0 g/L, mass ratio=1:20), and (c) feeding dosage (ball-milling time: 4 h, mass ratio=1:20). (pH=6.1, $[NB]_0$=100 mg/L, 25 °C)

Fig. S14. Effects of common substances on the NB removal efficiencies by Fe–N–C/ZVI and mZVI: (a) chloride, (b) sulfate, (c) bicarbonate, (d) humic acid ($[NB]_0$=100 mg/L, T=298 K, pH=5.0, reaction time=120 min).

Fig. S15. Comparative evaluation of NB removal efficiency and kinetic behavior under varying pH conditions. Subfigure pairs (a-b) pH=3, (c-d) pH=5, (e-f) pH=7, and (g-h) pH=9 show temporal removal profiles (left panels) and corresponding kinetic fittings (right panels), respectively. ($[NB]_0$=100 mg/L, T=298 K).

Fig. S16. The cyclic fixed-bed decontamination performances of Fe–N–C, mZVI, and Fe–N–C/ZVI toward (a) synthesized wastewater and (b) real wastewater collected from an industrial park (T=298 K, flow rate=6 BV/h).

Fig. S17. The iron ion concentration was detected in the effluent from continuous-flow degradation experiments. ($[NB]_0$=60 mg/L, T=298 K, flow rate=6 BV/h).

Scheme S1. Proposed pathway for NB electrochemical reduction by Fe–N–C electrode.

Supplementary Text, Figures and Tables

Text S1. Electrochemical Analysis

(1) Preparation of coated glassy carbon electrode

A catalyst-coated glassy carbon electrode was prepared by dipping catalytic ink on the glassy carbon electrode (GCE). The catalyst powder (10 mg) was dispersed in a mixed solution containing 780 μL of water, 200 μL of ethanol, and 20 μL of Nafion (5 wt%) by 30-min ultrasonication. A volume of 10 μL of the resulting catalyst ink was drop-cast onto the glassy carbon (GC) electrode surface and then dried at room temperature. Before use, the GC electrode (Φ = 5 mm) was polished with 50 nm Al2O3 powder and then washed with deionized water.

(2) Electrochemical active surface area (ECSA) measurement

Various catalysts' electrochemical active surface area (ECSA) was determined by measuring the capacitive current associated with double-layer charging from the scan-rate dependence of CV curves. ECSA measurements were performed in a 0.5 M Na_2SO_4 electrolyte using a three-electrode setup, with a Pt plate as the counter electrode, an Ag/AgCl electrode as the reference, and a catalyst-coated GCE as the working electrode. The CV measurements were conducted within a potential window of 0.3-0.4 V vs. Ag/AgCl, and the scan rates employed were 20, 40, 60, 80, and 100 mV s^{-1}. The double-layer capacitance (C_{dl}) of each catalyst was obtained by plotting the difference between the anodic and cathodic current densities at 0.35 V *vs.* Ag/AgCl against the scan rate. The slope of this linear plot corresponds to twice the double-layer capacitance (C_{dl}), which serves as a proxy for the ECSA.

Text S2. Fabrication of self-supported Fe–N–C electrode

Self-supported PTFE membrane electrodes were fabricated using a casting method for the reduction of nitrobenzene (NB). The electrode composition comprised the as-synthesized catalyst as the active material, carbon black (CB) as the conductive agent, and polytetrafluoroethylene (PTFE, 10 wt% aqueous dispersion) as the binder. These components were homogenized in a mass ratio of 8:1:1 (catalyst: CB: 10 wt% PTFE) under sequential ultrasonication (30 min) and mechanical stirring. Anhydrous ethanol was incrementally added during stirring to promote fibrillation, resulting in a cohesive, agglomerated paste. The paste was then uniformly roll-pressed onto a titanium (Ti) mesh current collector using a heated roller system (120 °C) to form the PTFE membrane electrode. The resulting electrodes exhibited an active material loading density of 4.7~5.0 $mg \cdot cm^{-2}$.

Text S3. Nitrobenzene reduction by Fe–N–C /ZVI composite

Batch reduction experiments were conducted in a 60 mL amber glass reactor under ambient aerobic conditions. The reaction system contained 50 mL of nitrobenzene (NB) solution (100 $mg \cdot L^{-1}$ prepared by diluting a stock solution (1 $g \cdot L^{-1}$), with initial pH maintained at 6.1±0.1 without buffer addition. For each trial, 0.05 g of zero-valent iron (ZVI) or Fe–N–C/ZVI composite was introduced into the reactor under constant magnetic stirring (600 rpm). Aliquots (0.5 mL) were periodically withdrawn, immediately filtered through 0.45 μm polyethersulfone (PES) membranes, and stored at 4 °C for subsequent analytical characterization. The pH of the solution was adjusted to predetermined values (3.0-9.0) to evaluate the effects of pH using 1 M HCl or NaOH solutions. All experiments were performed in triplicate with parallel controls at 25°C.

Text S4. Continuous-flow degradation experiment

Fixed-bed degradation experiments were conducted in a glass column (300 mm length, 20 mm diameter) filled with 5 mL of wet Fe–N–C/ZVI. Both synthetic and real wastewater, collected from an industrial park containing approximately 60 mg/L of NB and other competing anions, were fed into the columns using a constant-flow peristaltic pump. The empty bed contact time (EBCT) for these experiments was set to 10 minutes, corresponding to a flow rate of 6 bed volumes per hour (BV/h). After the degradation process, the effluent was collected and analyzed for further evaluation.

Text S5. Quantification of nitrobenzene (NB) and aniline (AN) by HPLC.

Residual nitrobenzene (NB) and aniline (AN) concentrations in treated wastewater were quantified using high-performance liquid chromatography (HPLC) under the following operational parameters: Column: C18 reverse-phase column (250 mm × 4.6 mm, 5 μm particle size); Detection: UV absorbance at 254 nm; Mobile phase: Methanol/water (60:40, v/v); Flow rate: 1.00 $mL \cdot min^{-1}$; Column temperature: 35 °C; Injection volume: 30 μL. Chromatographic separation yielded distinct retention times of 3.2 min for AN and 7.8 min for NB. Calibration curves (Fig. S1) were established using serially diluted standard solutions (5-120 $\mu g \cdot mL^{-1}$), demonstrating excellent linearity: AN: C=8.30462 A+ 0.32314 (R^2=0.9999), and NB: C=0.86998 A + 0.93677 (R^2=0.9997). Where C represents concentration ($\mu g \cdot mL^{-1}$), and A corresponds to the chromatographic peak area. All samples were filtered through 0.45 μm PES membranes before injection.

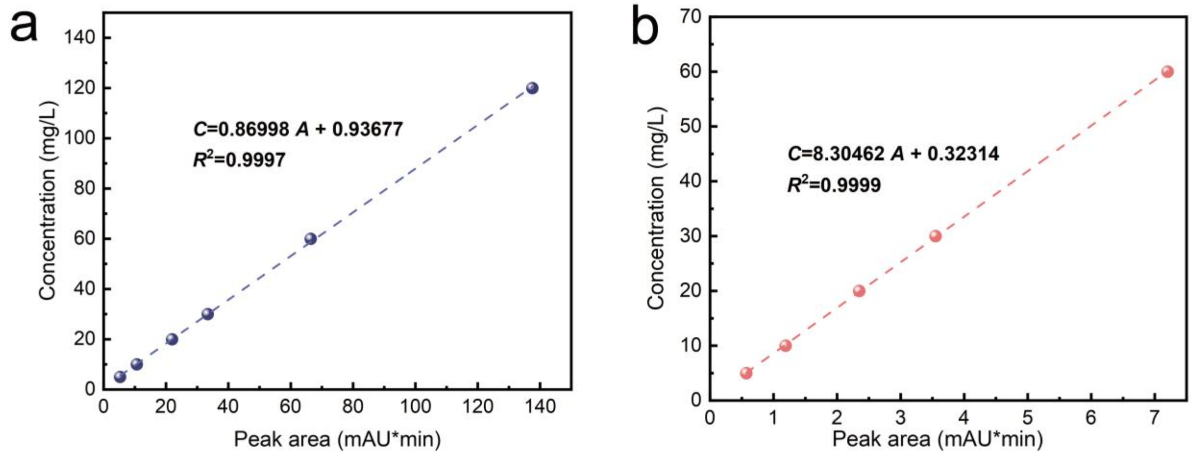

Fig. S1. Calibration curves for the quantification of (a) nitrobenzene (NB) and (b) aniline (AN) by HPLC.

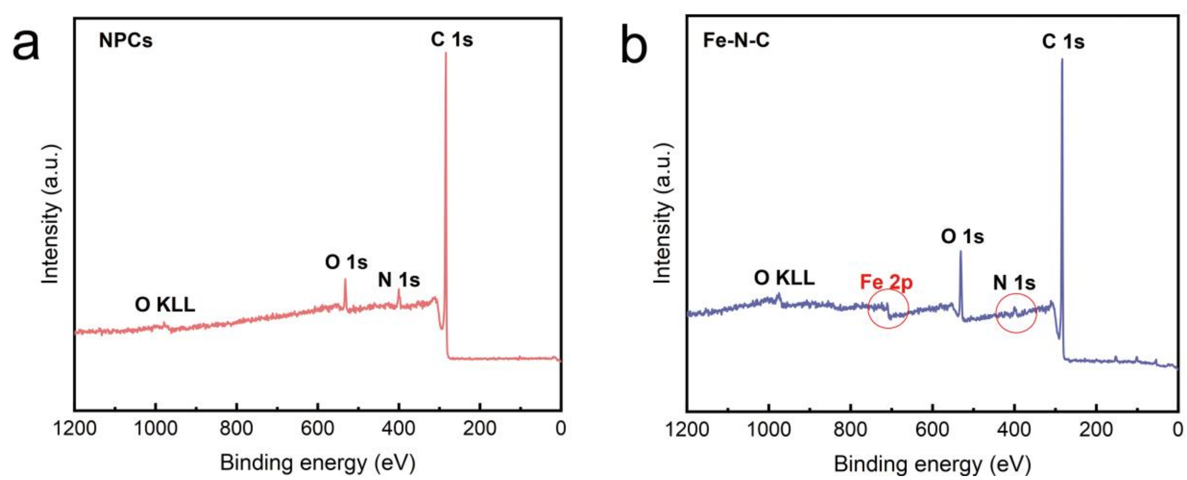

Fig. S2. Survey XPS spectra of (a) NPCs and (b) Fe–N–C materials.

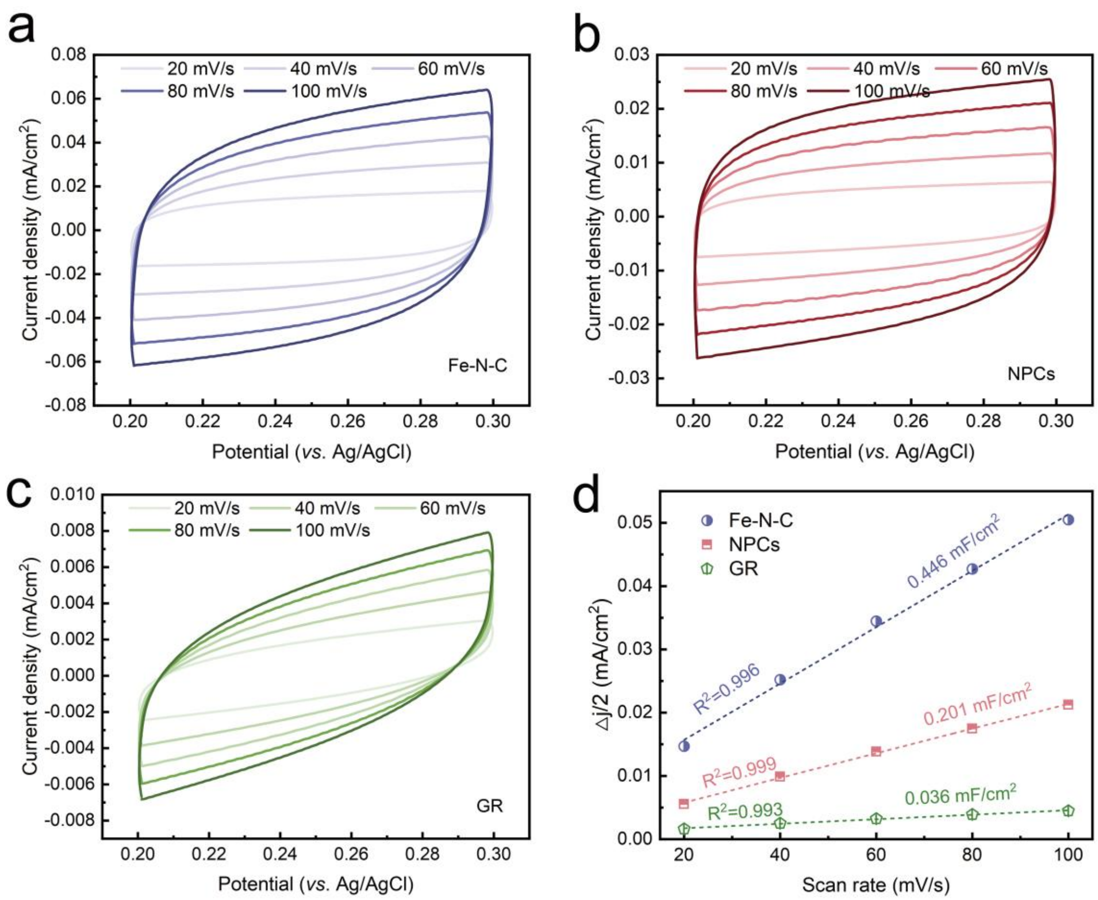

Fig. S3. CV curves of (a) Fe–N–C, (b) nitrogen-doped porous carbons (NPCs), (c) graphite (GR), and (d) ECSA measurements of catalysts based on the double-layer capacitance (C_{dl}) over a range of scan rates. (pH=7.0, $[Na_2SO_4]_0$=0.5 M, T=298 K).

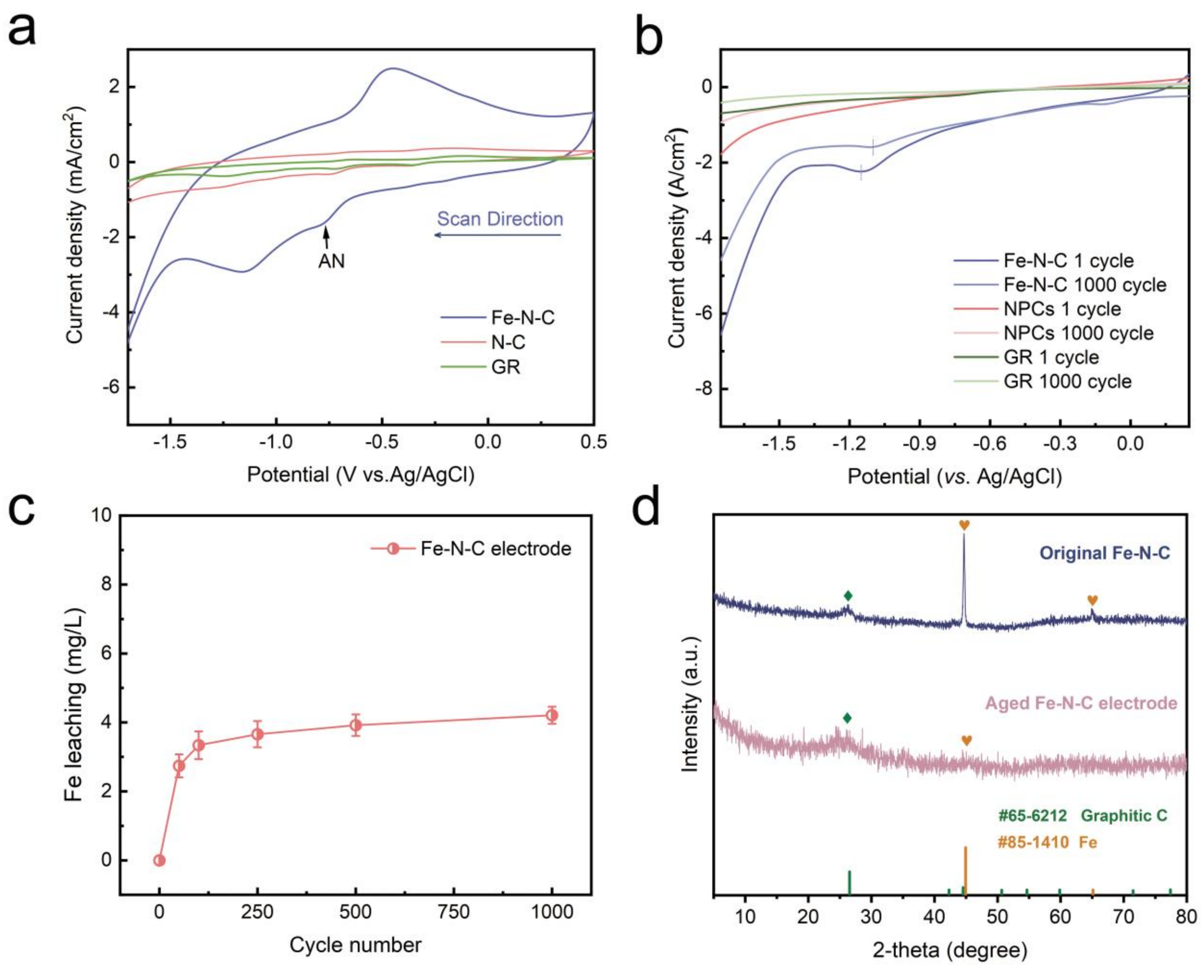

Fig. S4. Electrochemical performance and stability of different catalysts. (a) Cyclic voltammetry (CV) curves, and (b) cycling stability of Fe–N–C, NPCs, and GR electrodes. (c) Iron leaching observed during 1000 linear sweep voltammetry (LSV) cycles. (d) XRD patterns of the post-cycling Fe–N–C electrode. (Scan rate=50 mV/s, $[Na_2SO_4]_0$=50 mM, $[NB]_0$=100 mg/L).

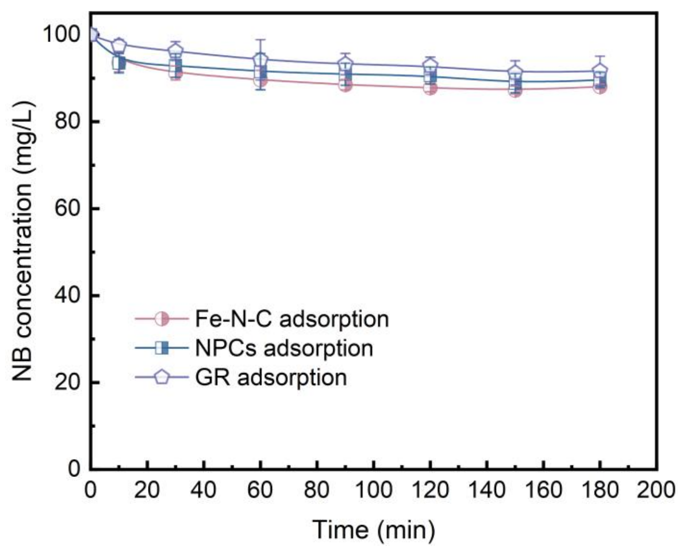

Fig. S5. Adsorption of nitrobenzene (NB) by electrodes prepared from active carbons (ACs), nitrogen-doped porous carbons (NPCs), and Fe–N–C. (pH=6.1, $[NB]_0$=100 mg/L, $[Na_2SO_4]_0$=50 mM, T=298 K).

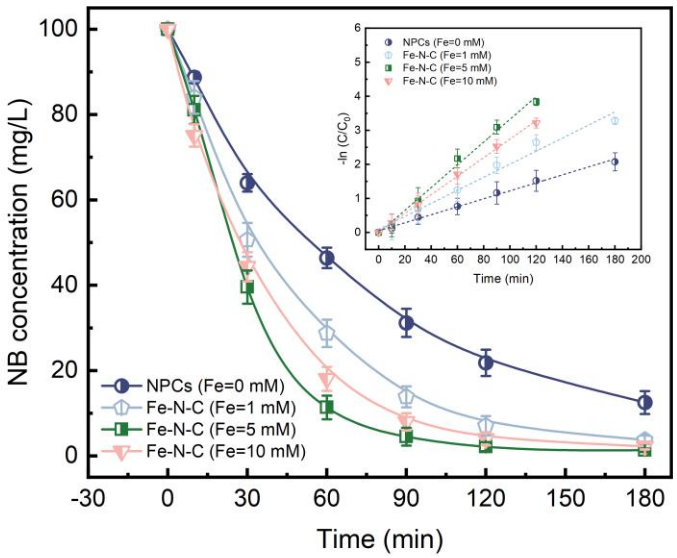

Fig. S6. Effect of iron content in Fe–N–C electrodes on the electrocatalytic performance of nitrobenzene (NB). (inset: pseudo-first-order kinetic fitting). Experimental conditions: pH=6.1, $[NB]_0$=100 mg/L, $[Na_2SO_4]_0$=50 mM, T=298 K.

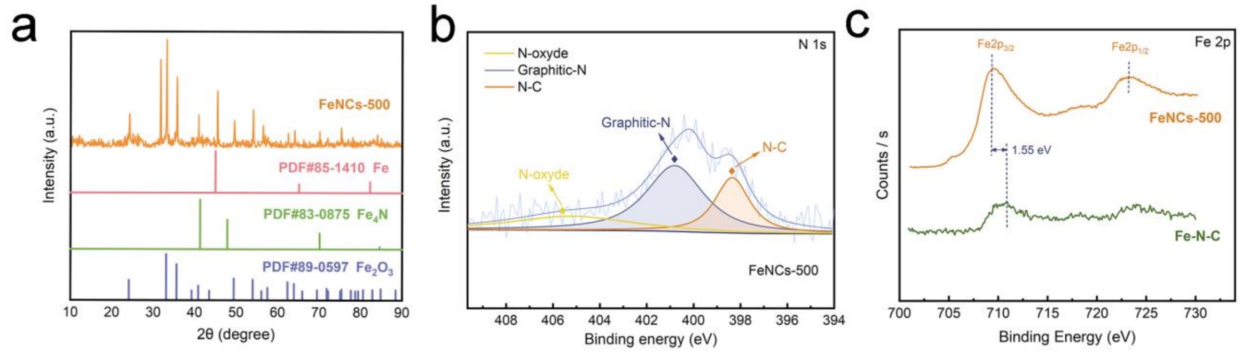

Fig. S7. Structural and compositional characterization of FeNCs-500 catalyst. (a) XRD patterns, and (b) high-resolution N 1s XPS spectra. (c) The Fe 2p narrow scan spectra of FeNCs-500 and Fe–N–C catalysts.

The synthesis protocol for FeNCs-500 is detailed in Section 2.3. XRD analysis revealed the predominant presence of iron trioxide crystalline phases in the catalyst matrix. Deconvolution of the N 1s XPS spectrum demonstrated that the low calcination temperature (500°C) resulted in incomplete nitrogen coordination, as evidenced by the absence of characteristic Fe–N_x bonding configurations typically observed in higher-temperature (800°C) pyrolyzed catalysts (Fe–N–C).

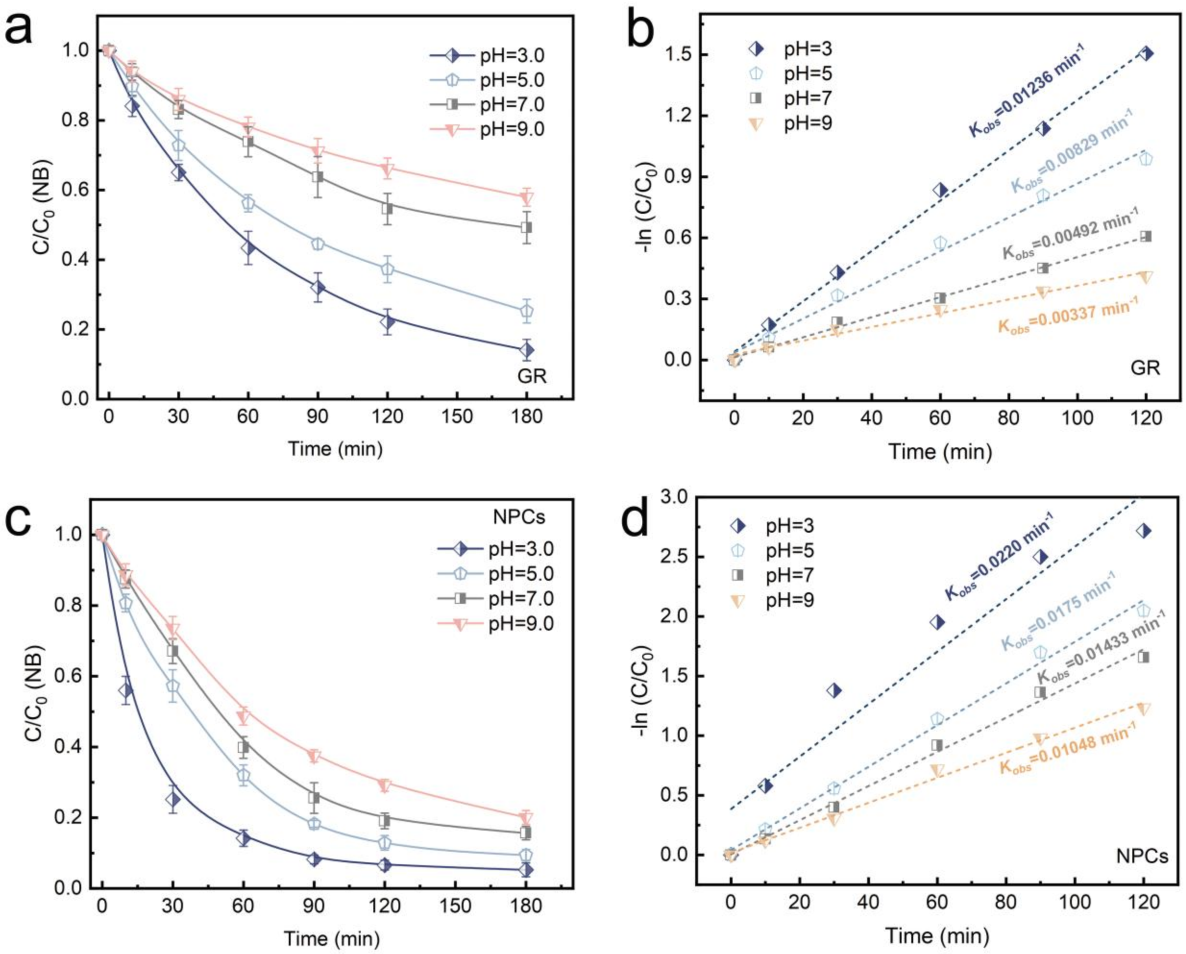

Fig. S8. Electrochemical reduction performance of NB using different electrocatalysts at varying pH conditions. (a) NB removal efficiency and (b) kinetics with GR electrode; (c) NB removal efficiency and (d) kinetics with NPCs electrode. (T=298 K, $[NB]_0$=100 mg/L, $[Na_2SO_4]_0$=50 mM, potential=-1.0 V *vs*. Ag/AgCl).

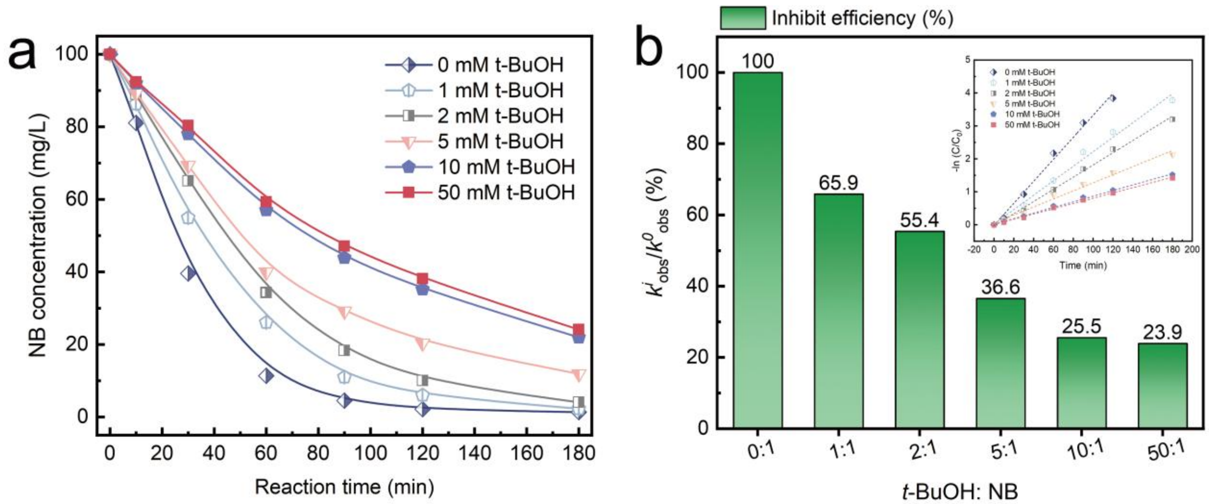

Fig. S9. (a) Reduction efficiency of NB and (b) its pseudo-first-order rate constant (k_{obs}) ratio on the Fe–N–C cathode with different *t*-BuOH concentrations (Potential=-1.0 V *vs*. Ag/AgCl, T=298 K, $[NB]_0$=100 mg/L, $[Na_2SO_4]_0$=50 mM, electrolysis time=180 min).

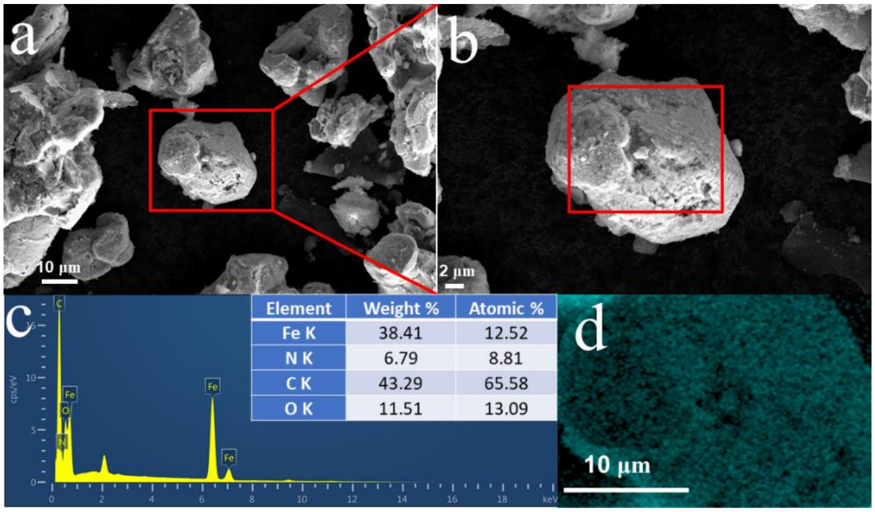

Fig. S10. Morphological and elemental characterization of Fe–N–C/ZVI. (a and b) FE-SEM images, (c) EDS elemental distribution, and (d) EDS elemental mapping images of Fe–N–C/ZVI. The inset of (c) shows the chemical composition of the samples.

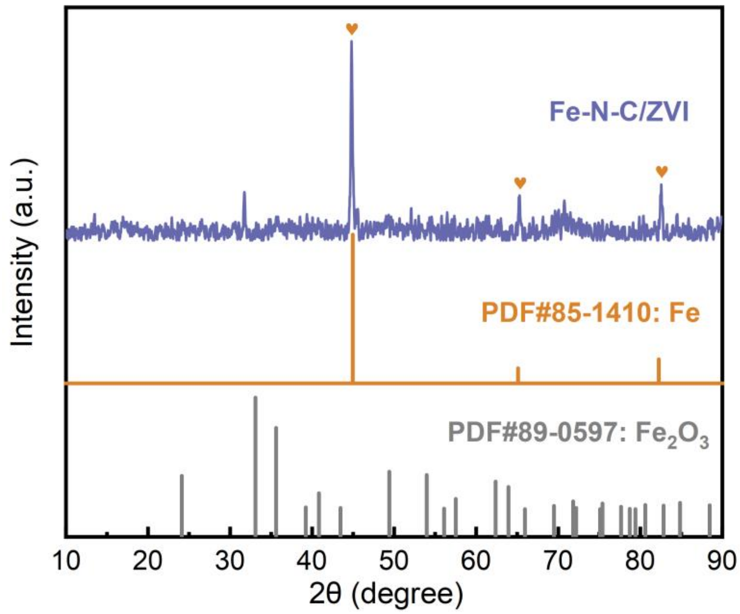

Fig. S11. XRD patterns of the Fe–N–C/ZVI composite as well as Fe (PDF#85-1410, yellow vertical line) and Fe_2O_3 (PDF#89-0597, black vertical line) as references.

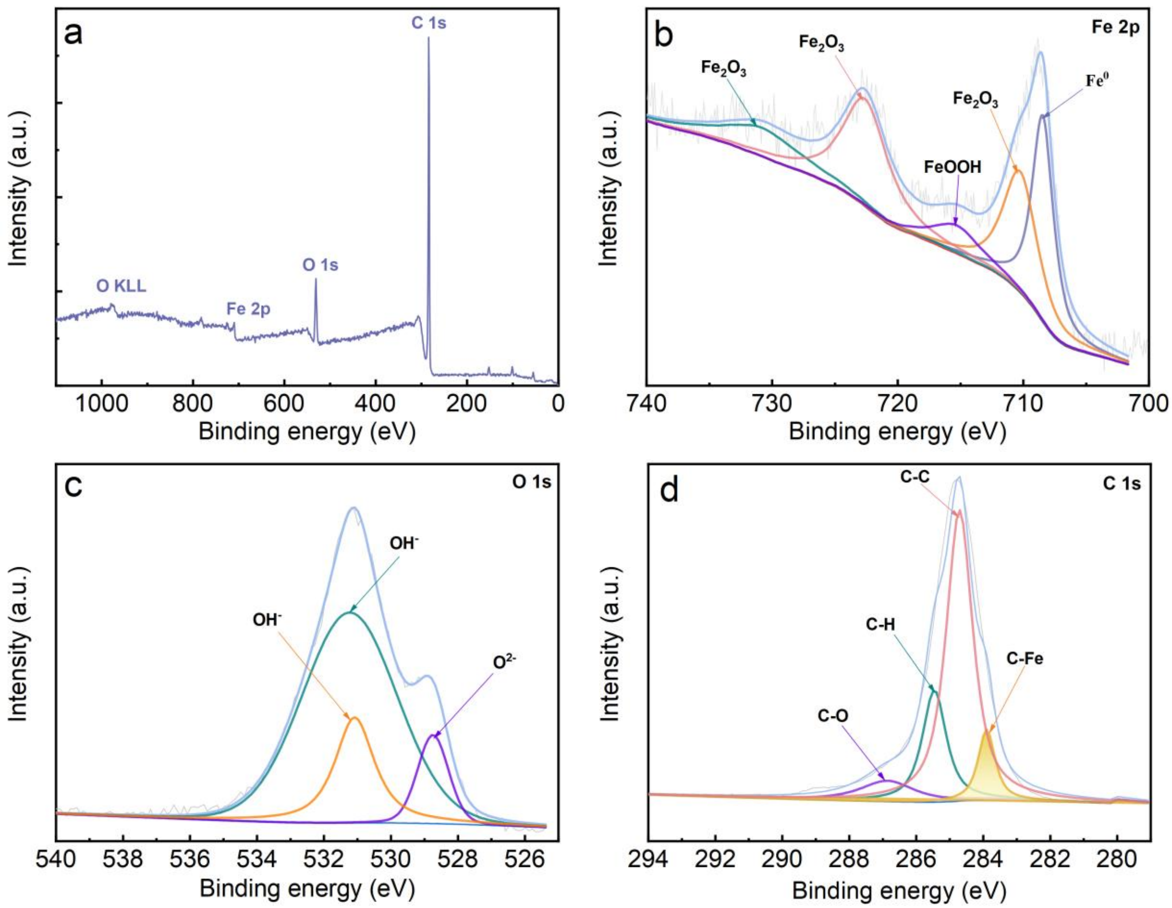

Fig. S12. High-resolution XPS spectra of (a) survey scan, (b) Fe 2p, (c) O 1s, and (d) C 1s for the Fe–N–C/ZVI composite.

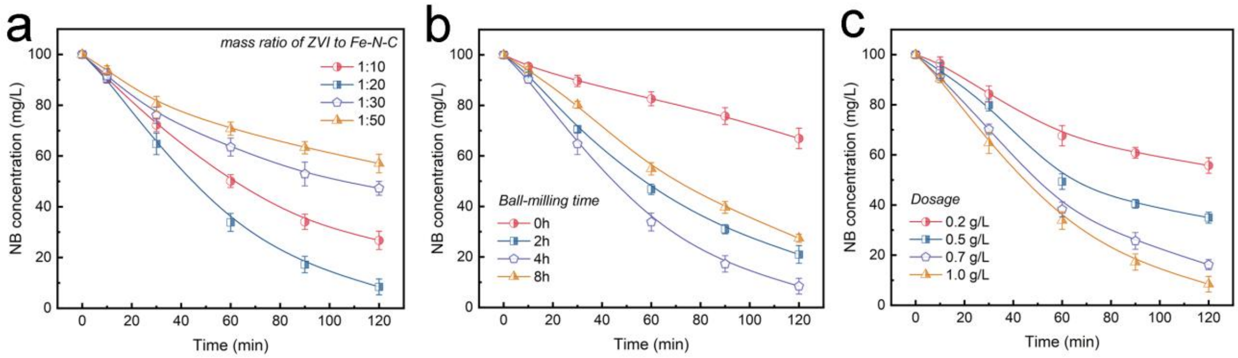

Fig. S13. Parametric optimization of Fe–N–C/ZVI composites for nitrobenzene (NB) degradation. (a) Effect of mZVI/Fe–N–C mass ratio ([dosage]=1.0 g/L, ball-milling time: 4 h), (b) Ball-milling duration ([dosage]=1.0 g/L, mass ratio=1:20), and (c) feeding dosage (ball-milling time: 4 h, mass ratio=1:20). (pH=6.1, $[NB]_0$=100 mg/L, 25 °C)

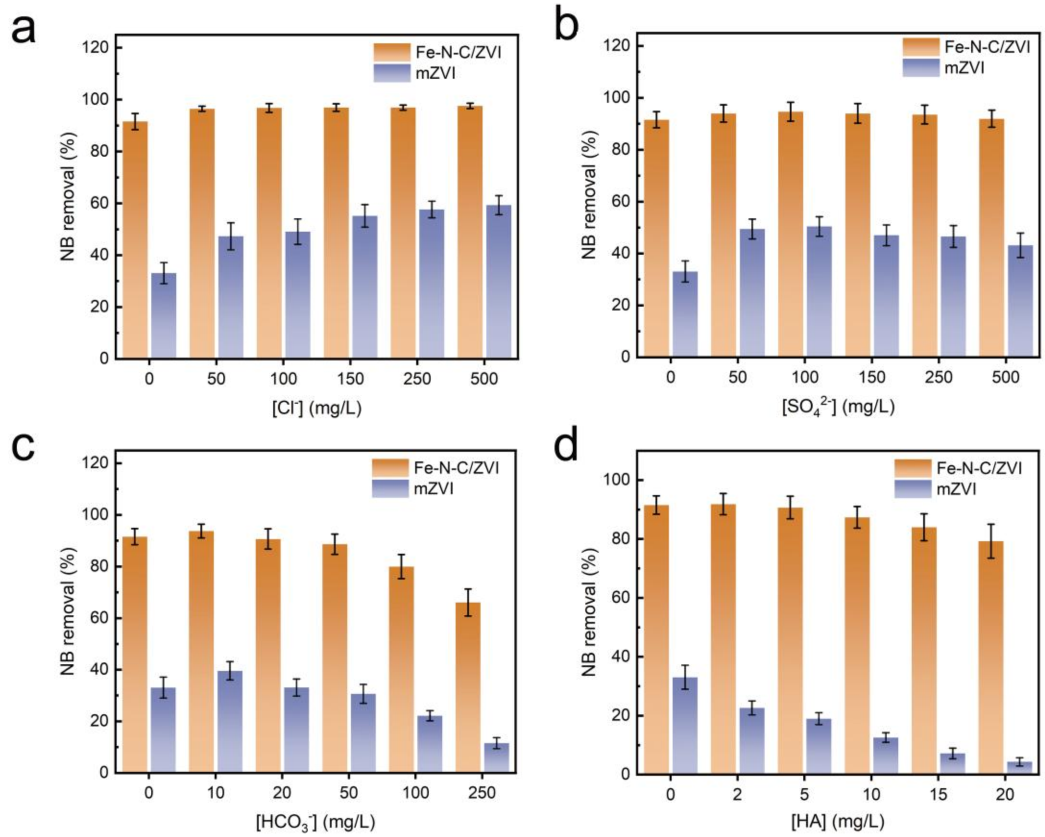

Fig. S14. Effects of common substances on the NB removal efficiencies by Fe–N–C/ZVI and mZVI: (a) chloride, (b) sulfate, (c) bicarbonate, (d) humic acid ($[NB]_0$=100 mg/L, T=298 K, pH=5.0, reaction time=120 min).

Note: As shown in Fig. S14a and S14b, the introduction of SO_4^{2-} and Cl^- slightly enhanced nitrobenzene (NB) removal, primarily due to their ability to disrupt the passivating oxides on the iron surface, thereby regenerating the active sites (Huang and Zhang, 2006; Wang et al., 2006). Fig. S14c indicates that low concentrations of bicarbonate (<50 mg/L) had negligible effects on both mZVI and Fe–N–C/ZVI. However, when the bicarbonate concentration was increased to 250 mg/L, the removal efficiency of both materials significantly decreased. This reduction is attributed to the formation of insulating iron carbonate precipitates (e.g., siderite) on the mZVI surface, which could retard the electron transportation (Yin et al., 2012). Moreover, although HA imposed impact on the decontamination efficiency of both materials, Fe–N–C/ZVI was relatively less affected than mZVI (Fig. S14d), which could be attributed to the fact that the modification of the Fe–N–C catalytic layer could effectively alleviate the inactivation of reaction sites that are usually caused by the quick complexation of macromolecular HA with iron species (Zhang et al., 2009). Given the prevalence of NOM in natural environments, Fe–N–C/ZVI is anticipated to offer superior decontamination stability and efficiency under realistic conditions.

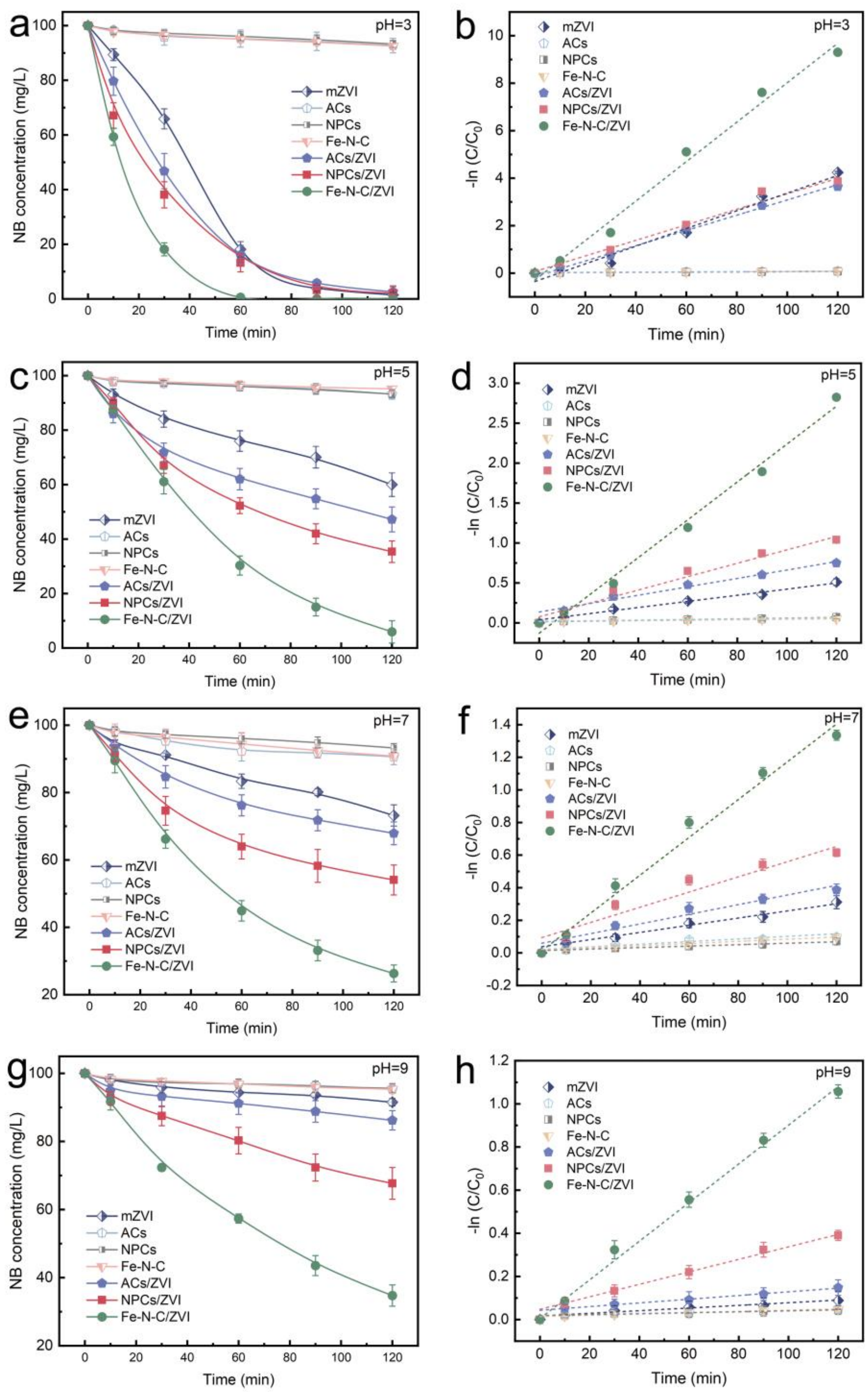

Fig. S15. Comparative evaluation of NB removal efficiency and kinetic behavior under varying pH conditions. Subfigure pairs (a-b) pH=3, (c-d) pH=5, (e-f) pH=7, and (g-h) pH=9 show temporal removal profiles (left panels) and corresponding kinetic fittings (right panels), respectively. ($[NB]_0$=100 mg/L, T=298 K).

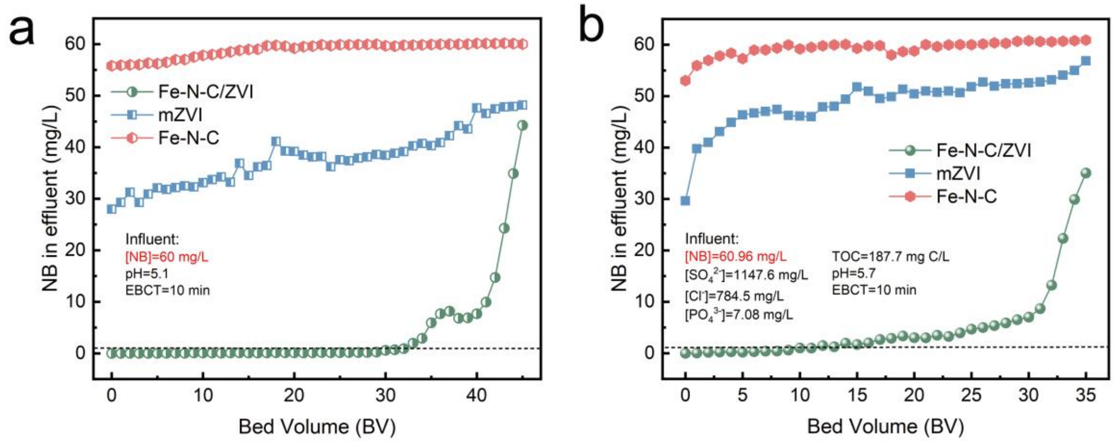

Fig. S16. The cyclic fixed-bed decontamination performances of Fe–N–C, mZVI, and Fe–N–C/ZVI toward (a) synthesized wastewater and (b) real wastewater collected from an industrial park (T=298 K, flow rate=6 BV/h).

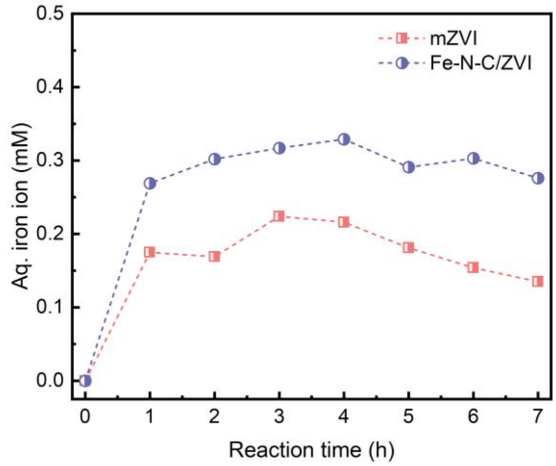

Fig. S17. The iron ion concentration was detected in the effluent from continuous-flow degradation experiments. ($[NB]_0$=60 mg/L, T=298 K, flow rate=6 BV/h).

Table S1. AC-impedance spectrum (EIS) fitting parameters for different catalysts.

Materials	R_s ($\Omega \cdot cm^2$)	R_{ct} ($\Omega \cdot cm^2$)	W_o-R ($\Omega \cdot cm^2$)	*error* (%)
Fe–N–C	0.507	0.124	0.1415	4.81
NPCs	0.829	1.053	2.421	3.56
GR	1.4	2.24	1.861	1.78

Table S2. GC–MS analysis of intermediates in the electrocatalytic reduction of nitrobenzene using Fe–N–C electrode.

Compound	Chemical formula	Molecular weight	Mass of predominant ions in the fragmentation pattern	Retention time (min)
Nitrobenzene (NB)	$C_6H_5NO_2$	123.11	51, 60, 65, 77, 87, 93, 107, 115, 123 (M^+)	16.96
Nitrosobenzene (NSB)	C_6H_5NO	107.11	51, 60, 63, 66, 74, 77, 107 (M^+)	12.36
Phenyl hydroxylamine (PHA)	C_6H_7NO	109.13	39, 51, 65, 66, 77, 80, 92, 93, 109 (M^+)	11.19
Aniline (AN)	$C_6H_5NH_2$	93.13	52, 55, 60, 63, 66, 74, 78, 90, 93 (M^+)	7.63
Azobenzene (AB)	$C_{12}H_{10}N_2$	182.22	51, 57, 63, 71, 77, 91, 105, 115, 128, 139, 152, 182 (M^+)	25.03

Table S3. Corrosion currents and potentials for different materials obtained from polarization curves via Tafel extrapolation.

Materials	E_{corr} (V, *vs* SCE)	i_{corr} ($\mu A/cm^2$)
mZVI	-0.413	5.724
ACs/ZVI	-0.501	5.910
NPCs/ZVI	-0.562	7.036
Fe–N–C/ZVI	-0.621	10.393

Table S4. Comparison of chemical and electrochemical systems used for nitrobenzene degradation.

Catalyst	Condition	pH	Concentration of NB	NB removal	Reduction rate	Ref
Nitrogen-doped porous carbon	-0.8 V *vs.* SCE	5.0	100 mg/L	94% (180 min)	0.0167 min^{-1}	(Zhao et al., 2020)
Graphite	-0.8 V *vs.* SCE	5.0	100 mg/L	47% (180 min)	0.004 min^{-1}	(Zhao et al., 2020)
Fe^0/PVA microspheres	0.2 g/L	6.0	1 M	89% (200 min)	0.0027 min^{-1}	(Bai et al., 2009)
C-dots@ZVI	2 g/L	5.0	50 mg/L	100% (120 min)	0.0596 min^{-1}	(Fan et al., 2021)
mZVI particle (1 mm)	20 g/L	3~9	0.066 mM	87.5% (240 min)	0.0185~0.0038 min^{-1}	(Dong et al., 2010)
TiO_2 NTAs	-1.2 V *vs.* SCE	5.2	300 mg/L	95% (120 min)	0.0242 min^{-1}	(Ahmadi and Wu, 2019)
CNT-modified PGE	-1.2 V *vs.* SCE	5.0	1 mM	95% (50 min)	/	(Li et al., 2007)
Electrolysis/biochar	5V (1 g/L)	5.8	100 mg/L	99.2% (120 min)	0.0181 min^{-1}	(Liu et al., 2020)
TiO_{2-x} single crystals	-1.2 V *vs.* SCE	6.0	10 mg/L	90% (60 min)	0.0375 min^{-1}	(Liu et al., 2016)
Nitrogen-doped diamond (NDD)	-0.9 V *vs.* SCE	6.0	100 mg/L	73.6% (150 min)	0.0155 min^{-1}	(Zhang et al., 2014)
Electrolysis/ redox mediator	0.04 V *vs.* RHE (1 mM PW12)	1.0	10 mM	100% (180 min)	0.0339 min^{-1}	(Liu et al., 2024)
Zn/Fe-modified biochar	2 V (1 g/L)	5.6	100 mg/L	94% (120 min)	0.0147 min^{-1}	(Liu et al., 2021)
Cu_2O NPs/ BiO_{2-x} NSs	10 mA/cm^2	7.0	100 mg/L	90% (30 min)	/	(Chen et al., 2022)
(FeCoNiCuZn)O /graphite	-1.7 V *vs.* Ag/AgCl	6.0	31 mg/L	90% (240 min)	0.0156 min^{-1}	(Márquez et al., 2023)
Fe–N–C	-1.0 V *vs.* Ag/AgCl	3~9	100 mg/L	95% (120 min)	0.0377~0.0232 min^{-1}	This work
Fe–N–C/mZVI	1 g/L	3~9	100 mg/L	100% (60 min)	0.021~0.009 min^{-1}	This work

Scheme S1. Proposed pathway for NB electrochemical reduction by Fe–N–C electrode.

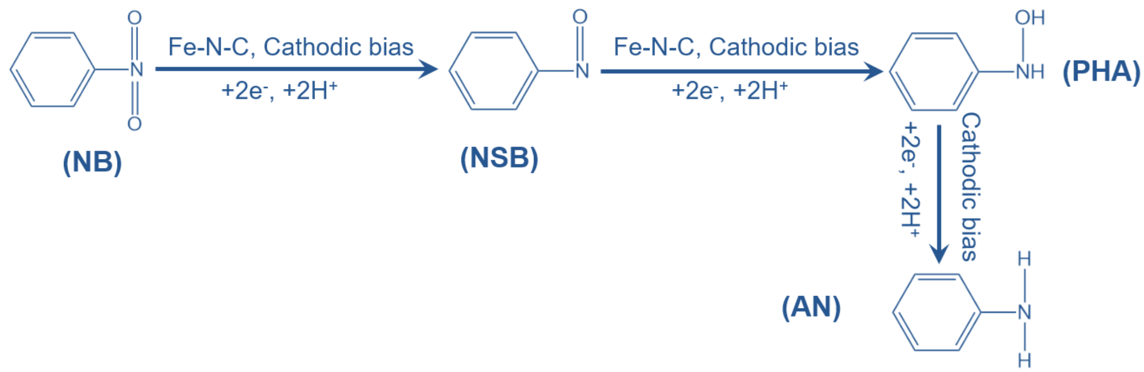

Reference

Ahmadi A, Wu T (2019). Electrocatalytic reduction of nitrobenzene using TiO2 nanotube electrodes with different morphologies: Kinetics, mechanism, and degradation pathways. Chemical Engineering Journal, 374: 1241-1252

Bai X, Ye Z-F, Qu Y-Z, Li Y-F, Wang Z-Y (2009). Immobilization of nanoscale Fe0 in and on PVA microspheres for nitrobenzene reduction. Journal Of Hazardous Materials, 172(2): 1357-1364

Chen M, Huang X, Wang N, Wang T, Yang J, Wei Y, Dao X, Zhou L, Hao H (2022). Cu2O nanoparticles modified BiO2-x nanosheets for efficient electrochemical reduction of nitrate-N and nitrobenzene from wastewater. Separation And Purification Technology, 289: 120728

Dong J, Zhao Y, Zhao R, Zhou R (2010). Effects of pH and particle size on kinetics of nitrobenzene reduction by zero-valent iron. Journal of Environmental Sciences, 22(11): 1741-1747

Fan P, Zhang X, Deng H, Guan X (2021). Enhanced reduction of p-nitrophenol by zerovalent iron modified with carbon quantum dots. Applied Catalysis B: Environmental, 285: 119829

Huang Y H, Zhang T C (2006). Reduction of nitrobenzene and formation of corrosion coatings in zerovalent iron systems. Water Research, 40(16): 3075-3082

Li Y-P, Cao H-B, Liu C-M, Zhang Y (2007). Electrochemical reduction of nitrobenzene at carbon nanotube electrode. Journal Of Hazardous Materials, 148(1): 158-163

Liu C, Zhang A-Y, Pei D-N, Yu H-Q (2016). Efficient Electrochemical Reduction of Nitrobenzene by Defect-Engineered TiO2–x Single Crystals. Environmental Science & Technology, 50(10): 5234-5242

Liu G-F, Zhang S, Chen C-J, Xing S-M, Zhang X-Y, Zhang Y-J, Wu D-Y, Li J-F, Ren B, Chen J-J (2024). Electrochemical Hydrogenation of Nitrobenzene: From Electrocatalysis to Redox Mediator Catalysis. Chemistry Of Materials, 36(18): 8825-8833

Liu Q, Bai X, Su X, Huang B, Wang B, Zhang X, Ruan X, Cao W, Xu Y, Qian G (2020). The promotion effect of biochar on electrochemical degradation of nitrobenzene. Journal Of Cleaner Production, 244: 118890

Liu Q, Jiang S, Su X, Zhang X, Cao W, Xu Y (2021). Role of the biochar modified with ZnCl2 and FeCl3 on the electrochemical degradation of nitrobenzene. Chemosphere, 275: 129966

Márquez V, Fereidooni M, Santos J S, Praserthdam S, Praserthdam P (2023). Evaluation of the hydrogenation reaction on the electrocatalytic nitrobenzene degradation over (FeCoNiCuZn)xOy high entropy oxides (HEOs). Chemosphere, 341: 140130

Wang W, Jin Z-H, Li T-L, Zhang H, Gao S (2006). Preparation of spherical iron nanoclusters in ethanol–water solution for nitrate removal. Chemosphere, 65(8): 1396-1404

Yin W, Wu J, Li P, Wang X, Zhu N, Wu P, Yang B (2012). Experimental study of zero-valent iron induced nitrobenzene reduction in groundwater: The effects of pH, iron dosage, oxygen and common dissolved anions. Chemical Engineering Journal, 184: 198-204

Zhang Q, Liu Y, Chen S, Quan X, Yu H (2014). Nitrogen-doped diamond electrode shows high performance for electrochemical reduction of nitrobenzene. Journal Of Hazardous Materials, 265: 185-190

Zhang Z, Cissoko N, Wo J, Xu X (2009). Factors influencing the dechlorination of 2,4-dichlorophenol by Ni–Fe nanoparticles in the presence of humic acid. Journal Of Hazardous Materials, 165(1): 78-86

Zhao X, Li A, Quan X, Chen S, Yu H, Zhang S (2020). Efficient electrochemical reduction of nitrobenzene by nitrogen doped porous carbon. Chemosphere, 238: 124636